Jiao, L., Truscott, B. S., Liu, H., Ashfold, M. N. R., & Ma, H. (2017). Imaging spectroscopy of polymer ablation plasmas for laser propulsion applications. Journal of Applied Physics, 121(1), [013303]. DOI: 10.1063/1.4973697

Imaging spectroscopy of polymer ablation plasmas for laser propulsion applications

Long Jiao, Benjamin S. Truscott, Hao Liu, Michael N. R. Ashfold, and Honghao Ma

Citation: J. Appl. Phys. **121**, 013303 (2017); doi: 10.1063/1.4973697
View online: http://dx.doi.org/10.1063/1.4973697
View Table of Contents: http://aip.scitation.org/toc/jap/121/1
Published by the American Institute of Physics

Imaging spectroscopy of polymer ablation plasmas for laser propulsion applications

Long Jiao,[1,2] Benjamin S. Truscott,[1] Hao Liu,[1] Michael N. R. Ashfold,[1] and Honghao Ma[2]
[1]*School of Chemistry, University of Bristol, Bristol BS8 1TS, United Kingdom*
[2]*CAS Key Laboratory of Mechanical Behavior and Design of Materials (LMBD), University of Science and Technology of China, Hefei 230027, China*

(Received 8 October 2016; accepted 21 December 2016; published online 6 January 2017)

A number of polymers have been proposed for use as propellants in space launch and thruster applications based on laser ablation, although few prior studies have either evaluated their performance at background pressures representative of the upper atmosphere or investigated interactions with ambient gases other than air. Here, we use spatially and temporally resolved optical emission spectroscopy to compare three polymers, poly(ethylene), poly(oxymethylene), and glycidyl azide polymer, ablated using a 532 nm, nanosecond pulsed laser under Ar and O_2 at pressures below 1 Torr. Emission lines from neutrally and positively charged atoms are observed in each case, along with the recombination radiation at the interaction front between the plasma plume and the background gas. C_2 radicals arise either as a direct fragmentation product or by a three-body recombination of C atoms, depending on the structure of the polymer backbone, and exhibit a rotational temperature of ≈5000 K. The Sedov–Taylor point blast model is used to infer the energy release relative to the incident laser energy, which for all polymers is greater in the presence of O_2, as to be expected based on their negative oxygen balance. Under Ar, plume confinement is seen to enhance the self-reactivity of the ejecta from poly(oxymethylene) and glycidyl azide polymer, with maximum exothermicity close to 0.5 Torr. However, little advantage of the latter, widely considered one of the most promising energetic polymers, is apparent under the present conditions over the former, a common engineering plastic. [http://dx.doi.org/10.1063/1.4973697]

I. INTRODUCTION

Pulsed laser ablation (PLA) finds widespread use in diverse applications, including pulsed laser deposition,[1] laser-induced breakdown spectroscopy,[2] surface modification,[3] and laser propulsion.[4] Relative to PLA in vacuum, additional physical processes occur in the presence of background gas, including shock wave creation and propagation,[5] plasma confinement,[6] and charge exchange during plasma formation and expansion. Many techniques have been employed to characterize the shock wave, including fast photography,[6] shadowgraphy,[7] interferometry,[8,9] time-gated emission imaging,[10,11] or spectroscopy.[12] Ablation of a broad range of materials has been investigated, spanning liquids to multi-component solid systems, under vacuum and in the presence of different pressures of both inert and reactive background gases, using a wide variety of laser types.[13–16] Laser ablation of polymers in low background pressures (≤1 Torr) has drawn relatively little attention, however, perhaps because of the complex physicochemical properties of polymer samples and the relatively low visibility of shock waves formed at low pressure.[9]

The promising performance of energetic or otherwise exothermic polymers in laser ablation propulsion applications[17–21] signals the need for a better understanding of the plumes produced by laser–polymer interactions in the presence of background gases of varying pressure and chemical nature. An understanding of the properties of the plasma plume and its interaction with the surrounding environment is key to envisioned space launches using ground-based lasers, for example, since the propulsive efficacy of the plume will be affected by the decline in ambient pressure with increasing altitude. Several previous investigations at (sea level) atmospheric pressure and in high vacuum have been reported,[22–24] but propulsion-focused laser ablation studies of polymers in low-pressure ambient gas, as is relevant to upper-atmosphere operation, are much rarer.[25] Such experiments also pertain to outer-space propulsion, since the physics of both the ablation event and the resulting shock, normally used to infer momentum transfer, are qualitatively different for a confined plume. We explore the PLA of three different polymers (detailed in Sec. II) using spatially and temporally resolved optical emission spectroscopy (OES) and time-gated emission imaging, with particular attention to shock wave formation and propagation

II. EXPERIMENT

The apparatus and experimental procedures have been described elsewhere.[26,27] All data presented here were obtained using just one ablation wavelength (532 nm) in the form of ≈100 mJ pulses (energy incident on the target, arriving at 45° angle of incidence) with durations of 6–7 ns (measured full width at half maximum, FWHM). The polymer targets, in the form of disks, were continuously rotated to limit cumulative damage, and a new disk was used for each experiment. The ablation chamber was evacuated to a

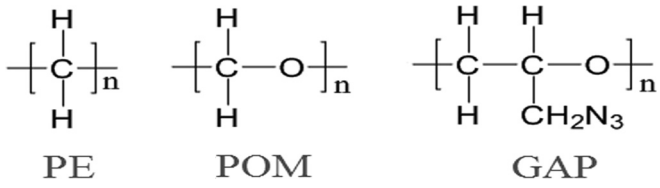

FIG. 1. Chemical structures of the three polymers investigated.

pressure $p \sim 10^{-2}$ Torr before introducing either argon or oxygen (representative non-reactive and reactive gases, respectively) through a mass flow controller, yielding background pressures of up to 1 Torr. Spatially resolved spectra of the plume emission in the range of $475 \leq \lambda \leq 520$ nm were captured for distances $0 \leq z \leq 6$ mm relative to the target surface, using a time-gated, intensified charge-coupled device (ICCD) camera attached to an imaging spectrograph, with the entrance slit parallel to the direction of plume expansion. A 532 nm notch filter was used to avoid unwanted detection of laser light, and images of the total emission from the plume (spectrally unresolved, 390–850 nm) could be recorded by replacing the diffraction grating in the spectrograph with a mirror. Measurements were made using a 10 ns gate width, at times across the range $0 \leq t \leq 2000$ ns after the peak of the laser pulse arriving at the target. As noted previously,[26,27] the use of such a short gate width ensures that the plume can be considered quasi-stationary during the observation period.

The polymers investigated were ultra-high molecular weight poly(ethylene) (PE), poly(oxymethylene) (POM), and glycidyl azide polymer (GAP), all in their natural form and without fillers or plasticizers. PE and POM are stiff, white materials, readily available commercially. GAP, a soft yellow elastomer, was prepared using the isocyanate curant Desmodur N 100 (Covestro AG, Leverkusen, Germany) following the process described by Sun and Li.[28] The chemical structures of these polymers are shown in Fig. 1. PE was chosen as a reference material, the thermochemical decomposition of which could be expected to be maximally exothermic in the presence of excess oxygen, and also the most endothermic under inert gas. POM is widely used in laser propulsion studies because of its relatively high specific impulse under, for example, CO_2 laser ablation.[18] GAP is a so-called energetic polymer and is currently viewed as one of the most promising candidate materials for laser micropropulsion.[17,21] A fluence $\Phi \approx 60$ J cm^{-2} (laser spot diameter $d \approx 500$ μm) was used for the ablation of POM and PE, whereas $\Phi \approx 120$ J cm^{-2} ($d \approx 350$ μm) was employed for GAP to compensate for its higher ablation threshold. The large values of Φ employed here, above the plasma threshold, were chosen to ensure maximal energy deposition and a strong shock, both in order to minimize the influence of varying optical properties between the materials and so that the Sedov–Taylor solution for an adiabatic point blast could be properly applied in the analysis.

III. RESULTS AND DISCUSSION

A. Polymer-dependent effects

Fig. 2 shows spatially resolved emission spectra and total emission images measured using a 10 ns gate width at $t = 40$ ns following 532 nm PLA of the three polymers in vacuum ($p \sim 10^{-2}$ Torr). The emitting material has visibly split into two components by this time, one of which is expanding rapidly, while the other remains near to the target surface. The wavelength-resolved images identify the atomic and molecular contributors to the total emission, and the observed species show obvious correlations with the chemical structure of the precursor polymer. Comparing the spectra of the various plumes, that of PE is dominated by atomic emissions from H_β and C (e.g., C I at 493.2 and 505.2 nm, and C II at 513.3, 514.4, and 515.1 nm) in this spectral range, while POM and GAP additionally show O II emissions (486.9, 489.1, 490.7, 492.4, 494.1, and 495.5 nm). N II lines (in the range 498–504 nm) are also apparent in the GAP plume emission, the strongest of which (~501 nm) also appear weakly, as an impurity, in panel (a). All line assignments were obtained from the NIST Atomic Spectra Database.[29] $C_2(d^3\Pi_g–a^3\Pi_u,$

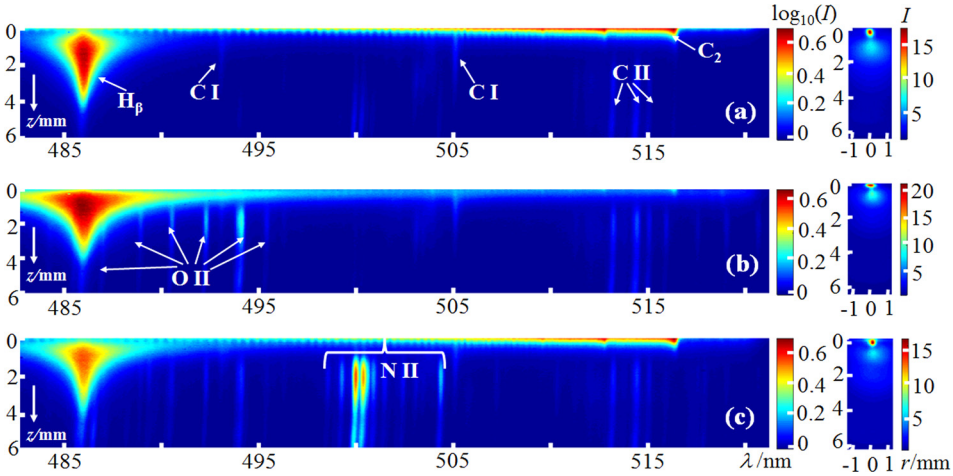

FIG. 2. Spatially resolved, wavelength- (λ-)dispersed (left) and total (right) emission images measured at $t = 40$ ns following 532 nm PLA of (a) PE, (b) POM, and (c) GAP under vacuum ($p \sim 10^{-2}$ Torr). The target surface is located at $z = 0$ mm, and the horizontal axis in the right hand images spans the range $-1 \leq r \leq 1$ mm in the plane orthogonal to z. The left- and right-hand images are displayed using logarithmic and linear false colour intensity (I) scales, respectively, which are shown to the immediate right of the images. Key emission features are identified in the wavelength-dispersed spectra.

$\Delta v = 0$) molecular emission (with the 0–0 band head at ≈517 nm, degraded to the blue) is clearly visible near the surface of the PE and GAP targets, but is very much weaker in the case of POM, reflecting the chemical composition of the respective polymers: PE is based on a chain of C atoms, whereas the backbones of GAP and POM consist of –CCO– and –CO– units, respectively. Intuitively, therefore, only from PE and GAP should one expect C_2 as a direct fragmentation product. The rotational structure of the C_2 emission extends beyond 485 nm. Comparison with spectral simulations using PGOPHER[30] and the spectroscopic constants given by Brooke *et al.*[31] suggests a minimal rotational temperature of ≈5000 K, which we take as representative of the near-surface gas temperature.

B. Ambient gas effects

In the presence of background gas at pressures $p \gtrsim 0.1$ Torr, the expanding ablation plume displaces the ambient medium and produces an adiabatic compression (blast) wave that propagates supersonically away from the target. A sufficiently strong shock is accompanied by continuum emission (principally due to recombination radiation) and can therefore be followed in a sequence of time-gated images. Figure 3 shows illustrative images measured in Ar and in O_2 at $t = 40$ ns. As energy is dissipated into the downstream gas, the shock velocity decreases toward the sound speed and the internal pressure approaches ambient, leading to a progressive slowing of the emission front and reduction in its intensity. With greater background pressure, this emission will be stronger, but the position of the shock front less advanced at any given time. The wavelength-dispersed spectra also reveal either Ar II lines when expanding into Ar, or (enhanced) O II emissions with O_2 as the background gas, which are observed with maximum intensity at the shock. However, the two gases differ in the spatial extent of their emission features: the Ar II lines extend beyond the band of continuum emission, whereas those of O II are more strongly confined within the shocked volume. With an initial temperature of several electron-volts, the principal constituents of the ablation plasma are neutral species (mostly atoms), electrons, and singly charged ions, the latter of which attain significantly higher velocities than the neutrals[11] and therefore carry much of the momentum of the expanding plume. The shock is produced primarily through the interaction of these ions with the neutral gas; indeed, Figs. 3(a) and 3(b) show C II emissions coincident with or slightly behind the shock front, with which they expand at a common velocity, while C I remains close to the target surface. The spatially extended Ar II lines thus probably originate from collisions with even more translationally excited multiplely charged ions (cf. Fig. 2), which are individually highly energetic but too few in number to contribute to shock formation. That the same is not observed for O II can be understood as the result of additional dissipative interactions applying to oxygen but not to argon, such as rotational and vibrational excitation, molecular dissociation, chemical reaction with

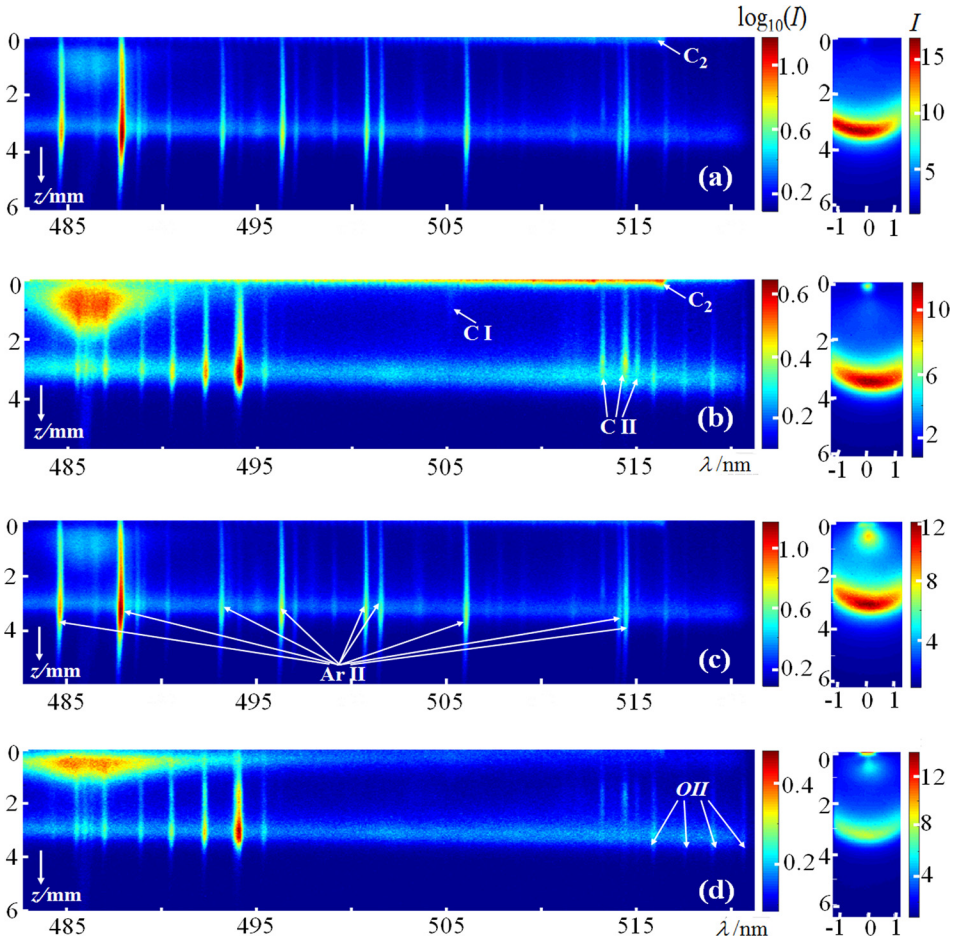

FIG. 3. Spatially resolved, wavelength-dispersed (left) and total (right) emission images measured at $t = 40$ ns following PLA of (a) PE in 0.5 Torr Ar, (b) PE in 0.5 Torr O_2, (c) POM in 0.5 Torr Ar, and (d) POM in 0.5 Torr O_2. Other details are as in Figure 2.

carbon and hydrogen ions, and so on. Such relaxation channels provide for excitation to be partitioned into other than electronic degrees of freedom, thus contributing to a relatively reduced fluorescence yield.

Compared to the emission spectra of PE in vacuum, the C I emission at small z appears relatively weaker in the presence of background O_2 (Fig. 3(b)). The corresponding emission is difficult to observe under Ar due to the intense Ar II lines. Later, $t \geq 120$ ns, a new band of C_2 emission arises at an intermediate position between the target surface and the shock, as shown in Fig. 4(a). Its time of appearance is independent of the identity of the background gas, and once visible, it appears to gain such speed (≈ 15 km s^{-1}) as to catch up with the shock front, shown in Fig. 4(b). The Ar II and O II emissions at small z (Figs. 3 and 4) indicate that the plasma plume interpenetrates the ambient gas rather than entirely displacing it, and so this fast-moving C_2 emission most likely arises via three-body recombination reactions $2(C\ I) + M \rightarrow C_2^* + M$, where C_2^* represents an emitting C_2 species and M = Ar or O_2 is a gas molecule. The observed $C_2(d^3\Pi_g)$ fragments may either be formed in this emitting state or arise via collisional/radiative relaxation from higher-lying states. The internal energies (2–3 eV) of these $C_2(d^3\Pi_g)$ species are much smaller than those needed to produce any of the relevant atomic emissions, leading to a greater relative contribution of C_2 to the total emission as the plasma temperature and density decline at later times.

The apparent acceleration and subsequent rapid propagation of the C_2 emission are less intuitive. We can envisage at least two plausible explanations. The first recognises that many of the precursor C atoms (or ions) are formed in highly excited states and thus need to experience a series of de-excitations (and/or electron captures) prior to recombining to yield the observed $C_2(d^3\Pi_g)$ products. Since the pressure and temperature are greatest near to the target, recombination occurs at first in this highly collisional environment, and only later in the sparser outer plume. The high apparent speed of the C_2 emission can then be accounted for as a phase velocity, rather than a group velocity, which is also consistent with its "spreading" z-profile, quite distinct from that of C_2 formed (and remaining) close to the origin. An alternative explanation for the progressive appearance of C_2 emission at longer distances from the target may be that all O_2 at a particular location is at first consumed through reaction with ablated C, C^+, etc., to form CO and CO_2 (which then become the collision partners), and the observed C_2 emission then emanates mainly from regions previously depleted in O_2. In this scenario, the expanding C_2 emission could indicate a combustion wave inside the shocked region.

B. Shock wave analysis

The Sedov–Taylor (S–T) self-similar point blast model is widely used to describe the propagation of a spherical shock wave. The S–T solution for the shock radius, R, is given by[32]

$$R = \varepsilon_0 \left(\frac{E}{\rho}\right)^{\frac{1}{5}} t^{\frac{2}{5}}, \tag{1}$$

where E is the total energy release that drives the shock wave, t is the time since the initiating event (here, the arrival of the laser pulse at the target), ρ is the ambient mass density and ε_0 is a constant that depends on the specific heat ratio, γ, of the gas and is given (to a sufficient approximation) by[32]

$$\varepsilon_0 = \left[\frac{75(\gamma-1)(\gamma+1)^2}{16\pi(3\gamma-1)}\right]^{\frac{1}{5}}. \tag{2}$$

The overall energy coupling efficiency can thus be obtained as the ratio, $\eta = E/E_0$, of the energy release required to produce an observed shock to the laser pulse energy, E_0. With sufficiently strong absorption of the incident radiation by the target material, η may approach unity, but only through its exothermic decomposition can this limit be exceeded.

Clearly, any evaluation of η rests on an accurate determination of R, but in practice the shock front is spatially blurred by the effects of viscosity, heat conduction, and so on, thereby departing from the ideal step discontinuity. Various methods have been proposed for determining the location of a shock front based on the leading edge of the

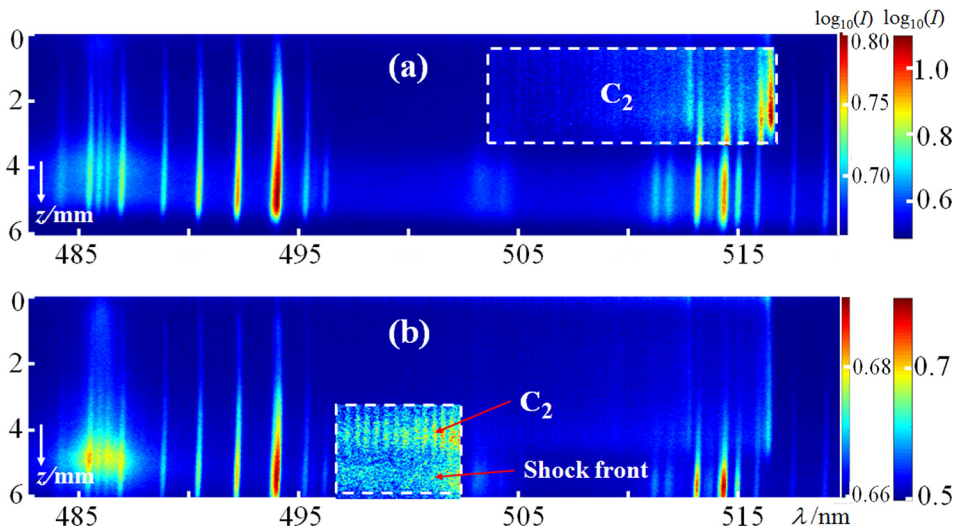

FIG. 4. Spatially resolved emission spectra measured at $t = $ (a) 150 ns and (b) 300 ns following PLA of PE under $p(O_2) = 0.8$ Torr. The main images are displayed using the logarithmic false colour intensity (I) scale shown at the far right of each image; the highlighted areas (bounded by the dashed rectangle) use the inner (expanded) intensity scale.

luminous front in an emission image,[11] e.g., by taking the position at which the emission intensity, I, reaches half of its peak value.[33] Assuming that emission intensity usefully reflects the underlying physical parameters, we have tested two measures, both proxies for rapid change in the local density and temperature: the point of half-maximum intensity, $R_{I,1/2}$, and that of maximum intensity gradient, $R_{g,\max}$, at the outermost rising edge of the I–z curve.

Figure 5(a) shows two plots of I vs. z for PLA of POM in $p(\mathrm{Ar}) = 0.5$ Torr, each recorded at $t = 40$ ns and normalised to peak intensity. The profile drawn in black shows emission in a ≈0.7 nm-wide band centred at 510 nm, away from any atomic emission feature (cf. Fig. 3) and therefore representing only recombination radiation, while the red curve is a cut through a total emission image along the target surface normal at the laser spot position, $(z, r = 0)$, as used in prior work.[34] The total emission decays less rapidly to large z due to spatially extended C II and Ar II lines that are poorly diagnostic of the shock position, but neither $R_{I,1/2}$ nor $R_{g,\max}$ is unduly sensitive to this potentially confounding long-range tail and the recovered values exhibit only a small dispersion. Figure 5(b) shows shock radii versus time by all four measures, again for POM under 0.5 Torr Ar, from which it can be seen that the power law exponent in each case remains sufficiently close to (although just above) the nominal value of $\frac{2}{5}$ expected from Eq. (1), despite the hemispherical geometry of the present blast waves. Hereafter, we exclusively employ $R = R_{g,\max}$ derived from the spectrally resolved data, both for the more direct physical interpretation these values support and because its correct determination does not rely (as does that of $R_{I,1/2}$) on the recorded emission intensity falling identically to zero ahead of the blast wave.

Figure 6 shows illustrative R–t curves for POM ablated under different pressures of Ar and O_2. The best-fit E values derived from these data are collected in Table I, along with the corresponding results for PE and GAP, the incident laser energy used in each experiment, and finally the inferred energy coupling efficiencies. The maximum pressure was limited to below 1 Torr in order to avoid the onset of the Rayleigh–Taylor instability and consequent turbulent mixing, which would render determinations of E unreliable. The use of the S–T model may overestimate E in certain cases,[5] most notable of which for the present experiments are if the flow velocity includes contributions from either adiabatic expansion of the plasma or further thermal ionization at the shock front. Since these effects will not differ much between the polymers, we focus primarily on the relative values of η.

POM and GAP return much higher energy coupling efficiencies under Ar than does PE, indicating contributions from chemical energy stored in these materials, whereas PE exhibits efficiencies always less than unity in the absence of oxygen. These trends are further examined in Fig. 7: η

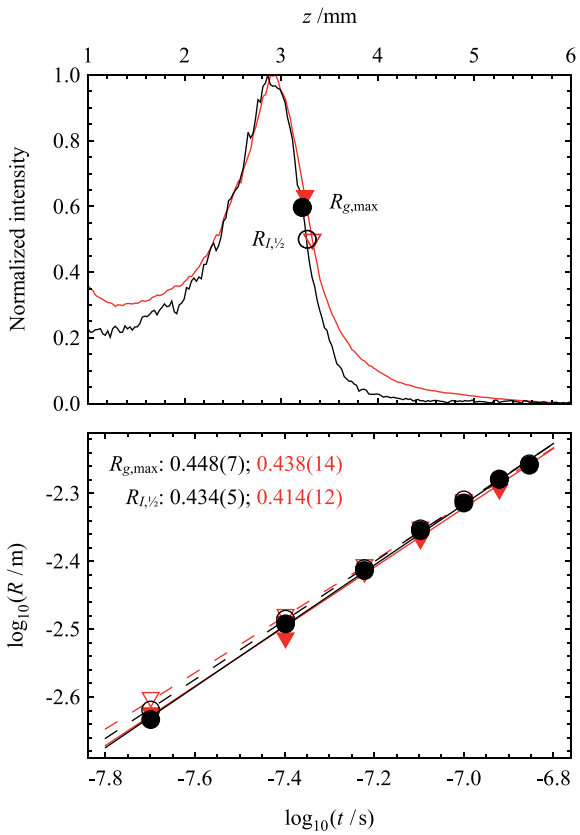

FIG. 5. (a) Illustration of $R_{I,1/2}$ and $R_{g,\max}$ in I–z plots obtained by monitoring either the total (red curve) or the 510 nm component of the wavelength-dispersed emission (black curve) at $t = 40$ ns following 532 nm PLA of POM in $p(\mathrm{Ar}) = 0.5$ Torr. (b) Double-logarithmic plot showing the t-dependence of the different measures of $R_{I,1/2}$ (open points and dashed line) and $R_{g,\max}$ (filled points and solid line), with the best-fit power law exponent and 1σ standard error (in parentheses) indicated in each case.

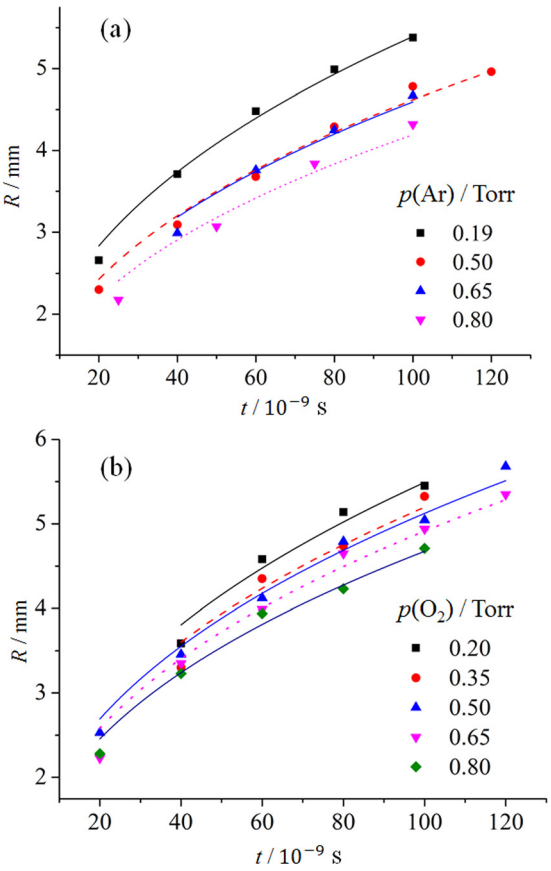

FIG. 6. R–t plots showing the shock position with respect to time after PLA of POM in different pressures of (a) Ar and (b) O_2. The continuous lines are best fits in terms of Eq. (1).

TABLE I. Shock energies and energy coupling efficiencies determined for 532 nm PLA of PE, POM, and GAP in different pressures ($p \leq 0.8$ Torr) of argon and oxygen. Figures in parentheses are 1σ standard (statistical) errors.

Polymer	Gas	p/Torr	E/mJ	E_0/mJ	η (%)
PE	Ar	0.25	72(11)	109(1)	66(10)
		0.50	55(14)	109(1)	51(13)
		0.65	34(9)	109(1)	31(8)
	O_2	0.20	147(17)	106(1)	139(16)
		0.50	279(12)	108(1)	258(11)
		0.65	389(7)	106(1)	368(7)
		0.80	383(12)	107(1)	358(12)
POM	Ar	0.50	129(8)	103(1)	126(8)
		0.65	165(12)	103(1)	160(12)
		0.80	130(12)	104(1)	124(12)
	O_2	0.20	160(13)	106(1)	151(12)
		0.50	263(16)	108(1)	244(15)
		0.65	277(24)	108(1)	257(22)
		0.80	266(18)	105(1)	253(17)
GAP	Ar	0.37	138(9)	111(1)	124(7)
		0.50	142(13)	108(1)	132(12)
		0.65	118(7)	108(1)	109(7)
	O_2	0.35	168(10)	107(1)	156(9)
		0.50	283(12)	106(1)	267(12)
		0.65	272(13)	106(1)	257(13)
		0.80	187(15)	108(1)	173(14)

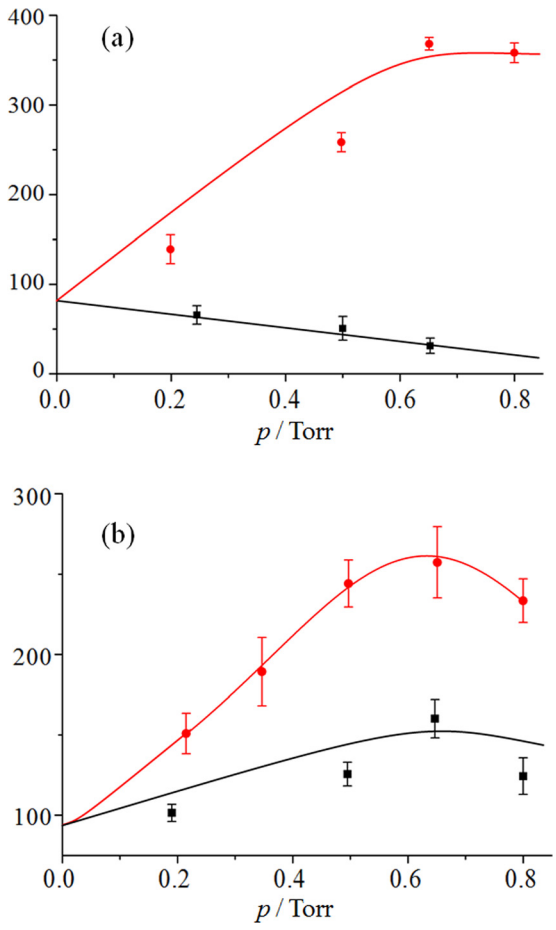

FIG. 7. Plots illustrating the variation of the energy coupling efficiency, η, with respect to p(Ar) (black) and $p(O_2)$ (red) following 532 nm PLA of (a) PE and (b) POM. The solid curves are merely indicative trend lines.

decreases with increasing p(Ar) for PE, while for POM it increases up to $p(\text{Ar}) \approx 0.65$ Torr, but declines with still higher pressure. This can be understood in terms of collision number, which scales with pressure: for a polymer lacking the possibility of self-reaction, collisions only serve to thermalize the ejecta and support the diffusion of heat into the ambient medium, reducing the energy coupling efficiency. Given exothermic self-reactivity, however, collisional thermalization of excess electronic excitation improves the reaction probability and hence is beneficial toward total energy release, in addition to increasing the frequency with which mutually reactive species encounter one another. Nevertheless, for background pressure above a critical value, unproductive collisions with Ar atoms begin to outweigh those between potential reactants, and heat transport to the surroundings becomes too rapid for complete reaction to occur. Clearly, the optimum pressure must depend on the polymer and the background gas, although the differences between POM and GAP appear modest by this measure.

The presence of ambient oxygen leads to a much-enhanced shock energy with all three polymers. As shown in Fig. 7(a), PE exhibits a remarkable ≈10-fold greater total energy release when ablated in $p(O_2) = 0.65$ Torr than under the same pressure of argon. As was observed with Ar, the energy coupling efficiency for POM in oxygen is seen to increase up to 0.65 Torr, then decline, as shown in Fig. 7(b); however, the limiting pressure for PE appears somewhat higher, >0.8 Torr. Again, this turn-over can be attributed to increasingly efficient thermalization, but since PE requires more external oxygen than does POM for its complete combustion, maximal exothermicity is achieved at higher pressure. Figure 8 compares the energy deposition following PLA of all three polymers into Ar and O_2 at $p = 0.5$ Torr. PE shows much the lowest coupling efficiency (at all pressures) in Ar, as expected for purely endothermic decomposition, but returns comparable values of η to POM and GAP when ablated in $p(O_2) = 0.5$ Torr.

PE and POM have similar physical and optical properties, and so the most significant difference between them for the present experiments is chemical, i.e., the presence of O atoms in the latter. The current study thus highlights the role of oxygen in enhancing the energy release on material ablation and isolates one aspect of the good performance afforded by POM in laser ablative propulsion. In contrast,

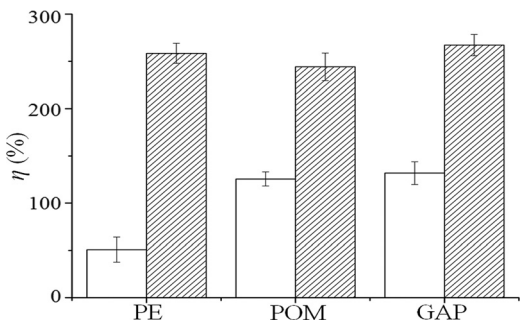

FIG. 8. Comparison of the energy coupling efficiencies, η, for the 532 nm PLA of PE, POM, and GAP under 0.5 Torr of both argon and oxygen (open and hatched bars, respectively).

much prior work has taken poly(vinyl chloride) (PVC), rather than PE, for comparison to other polymers;[4] however, the decomposition of PVC is not necessarily purely endothermic since the HCl product has a larger bond enthalpy than the C–Cl moiety in the polymer. The results shown in Fig. 8 can be rationalized in terms of oxygen balance: the surplus or deficit of oxygen, as weight percent, resulting from the complete combustion of each of the polymers to produce CO_2 and H_2O (and N_2, in the case of GAP).[35] The monomers of PE, POM, and GAP possess negative oxygen balance (−343%, −107%, and −121%, respectively), which accounts for their significantly better performance under ambient O_2; indeed, the status of PE as a pure fuel without any embodied oxygen enables a much larger maximal energy release in the reactive environment (cf. Table I) than for either of the other polymers. GAP is slightly more oxygen-deficient than POM, but the shock energy of GAP is compensated by the additional conversion of the azide group to N_2. Overall, POM and GAP yield similar results to one another, for both choices of the background gas.

IV. SUMMARY AND CONCLUSIONS

Spatially and temporally resolved optical emission spectroscopy has been used to study plasmas formed by 532 nm pulsed laser ablation of poly(ethylene), poly(oxymethylene), and glycidyl azide polymer targets in low background pressures ($10^{-2} \leq p \leq 1$ Torr) of both argon and oxygen. Atomic lines from each of the elements within the respective polymers are observed when ablating in vacuum ($p \sim 10^{-2}$ Torr). Emission from C_2 radicals is clearly observable near the surfaces of PE and GAP targets, but is much weaker in the case of POM, indicating a significant dependence of the products on the direct fragmentation of the polymer backbone. For higher pressures and at sufficiently late time, additional C_2 radical emission is observed further from (especially) the PE and GAP target surfaces, which reflects the recombination of C atoms in the presence of a third body, i.e., a gas molecule. The evolution of the apparent velocity of this secondary C_2 under O_2 may indicate a combustion wave propagating outwards within the shocked volume. The Sedov–Taylor point blast model has been applied to analyse the position of the blast wave and deduce the energy release from each polymer in relation to the laser pulse energy for a range of pressures. With all three materials, the availability of reactive oxygen leads to deflagration and thus to a much more exothermic decomposition, in line with expectations given the oxygen balance of the three substances. In an inert atmosphere, PE unsurprisingly yields much lower energy coupling efficiencies than either of the other polymers, but little distinction can be drawn between POM and GAP based on the present experiments despite the latter having widely been recognized as a promising energetic material.

ACKNOWLEDGMENTS

M.N.R.A and B.S.T. are grateful to EPSRC for the financial support via the Intelligent Manufacturing Initiative (EP/K018388/01). We are grateful to the China Scholarship Council for a visiting student scholarship to L.J., who further acknowledges the support from the National Natural Science Foundation of China (Grant Nos. 11302221 and 51374189), the Fundamental Research Funds for Central Universities (WK2480000002), and useful discussions with Professor Jian Cai (Institute of Microelectronics of the Chinese Academy of Sciences) and Dr. Long Li (Nanjing University of Science and Technology).

Raw data used in the preparation of this paper have been placed in the University of Bristol's research data repository and can be accessed using the DOI:10.5523/bris.1dxobtq9nyk1d1jv72ipiy7btl.

[1]*Pulsed Laser Deposition of Thin Films: Applications-Led Growth of Functional Materials*, edited by R. Eason (Wiley-Interscience, Hoboken, 2007).
[2]M. Banaee and S. H. Tavassoli, "Discrimination of polymers by laser induced breakdown spectroscopy together with the DFA method," Polym. Test. **31**, 759 (2012).
[3]T. Lippert, "Interaction of photons with polymers: from surface modification to ablation," Plasma Process. Polym. **2**, 525 (2005).
[4]C. Phipps, M. Birkan, W. Bohn, H. A. Eckel, H. Horisawa, T. Lippert, M. Michaelis, Y. Rezunkov, A. Sasoh, W. Schall, S. Scharring, and J. Sinko, "Review: Laser-ablation propulsion," J. Propul. Power **26**, 609 (2010).
[5]S. H. Jeong, R. Greif, and R. E. Russo, "Propagation of the shock wave generated from excimer laser heating of aluminium targets in comparison with ideal blast wave theory," Appl. Surf. Sci. **127–129**, 1029 (1998).
[6]D. B. Geohegan, "Fast intensified-CCD photography of $YBa_2Cu_3O_{7-x}$ laser ablation in vacuum and ambient oxygen," Appl. Phys. Lett. **60**, 2732 (1992).
[7]C. Porneala and D. A. Willis, "Time-resolved dynamics of nanosecond laser-induced phase explosion," J. Phys. D: Appl. Phys. **42**, 155503 (2009).
[8]T. Ditmire, K. Shigemori, B. A. Remington, K. Estabrook, and R. A. Smith, "The production of strong blast waves through intense laser irradiation of atomic clusters," Astrophys. J. Suppl. Ser. **127**, 299 (2000).
[9]P. Hough, T. J. Kelly, C. Fallon, C. McLoughlin, P. Hayden, E. T. Kennedy, J. P. Mosnier, S. S. Harilal, and J. T. Costello, "Enhanced shock wave detection sensitivity for laser-produced plasmas in low pressure ambient gases using interferometry," Meas. Sci. Technol. **23**, 125204 (2012).
[10]S.-B. Wen, X. L. Mao, R. Greif, and R. E. Russo, "Laser ablation induced vapor plume expansion into a background gas. II. Experimental analysis," J. Appl. Phys. **101**, 023115 (2007).
[11]S. S. Harilal, C. V. Bindhu, M. S. Tillack, F. Najmabadi, and A. C. Gaeris, "Internal structure and expansion dynamics of laser ablation plumes into ambient gases," J. Appl. Phys. **93**, 2380 (2003).
[12]M. Hauer, D. J. Funk, T. Lippert, and A. Wokaun, "Time-resolved techniques as probes for the laser ablation processes," Opt. Lasers Eng. **43**, 545 (2005).
[13]R. Fardel, L. Urech, T. Lippert, C. Phipps, J. M. Fitz-Gerald, and A. Wokaun, "Laser ablation of energetic polymer solutions: effect of viscosity and fluence on the splashing behaviour," Appl. Phys. A **94**, 657 (2009).
[14]S. Abdelli-Messaci, T. Kerdja, A. Bendib, and S. Malek, "CN emission spectroscopy study of carbon plasma in nitrogen environment," Spectrochim. Acta B **60**, 955 (2005).
[15]S. S. Harilal, "Expansion dynamics of laser ablated carbon plasma plume in helium ambient," Appl. Surf. Sci. **172**, 103 (2001).
[16]S. Choi, T. Han, A. B. Gojani, and J. J. Yoh, "Thrust enhancement via gel-type liquid confinement of laser ablation of solid metal propellant," Appl. Phys. A **98**, 147 (2010).
[17]C. Phipps, J. Luke, and T. Lippert, "Laser ablation of organic coatings as a basis for micropropulsion," Thin Solid Films **453–454**, 573 (2004).
[18]J. E. Sinko and A. Sasoh, "Review of CO2 laser ablation propulsion with polyoxymethylene," Int. J. Aerosp. Innovations **3**, 93 (2011).
[19]A. A. Ageichik, E. V. Repina, Yu. A. Rezunkov, and A. L. Safronov, "Detonation of CHO working substances in a laser jet engine," Tech. Phys. **54**, 402 (2009).
[20]L. Jiao, J. Cai, H. H. Ma, G. X. Li, L. Li, Z. W. Shen, and Z. P. Tang, "Research on applications of rectangular beam in micro laser propulsion," Appl. Surf. Sci. **301**, 481 (2014).

[21]L. Jiao, J. Cai, H. H. Ma, Z. W. Shen, L. Li, and Z. P. Tang, "Application of energetic materials in laser ablative micropropulsion," Int. J. Energ. Mater. Chem. Propul. **14**, 57 (2015).
[22]M. Hauer, D. J. Funk, T. Lippert, and A. Wokaun, "Time resolved study of the laser ablation induced shockwave," Thin Solid Films **453–454**, 584 (2004).
[23]L. Urech, T. Lippert, C. R. Phipps, and A. Wokaun, "Polymers as fuel for laser-based microthrusters: An investigation of thrust, material, plasma and shockwave properties," Appl. Surf. Sci. **253**, 7646 (2007).
[24]F. C. De Lucia, Jr. and J. L. Gottfried, "Influence of molecular structure on the laser-induced plasma emission of the explosive RDX and organic polymers," J. Phys. Chem. A **117**, 9555 (2013).
[25]W. O. Schall, H.-A. Eckel, W. Mayerhofer, W. Riede, and E. Zeyfang, "Comparative lightcraft impulse measurements," Proc. SPIE **4760**, 908 (2002).
[26]H. Liu, B. S. Truscott, and M. N. R. Ashfold, "Position- and time-resolved Stark broadening diagnostics of a non-thermal laser-induced plasma," Plasma Sources Sci. Technol. **25**, 015006 (2016).
[27]B. S. Truscott, Ph.D. thesis, University of Bristol, 2013.
[28]Y. L. Sun and S. F. Li, "The effect of nitrate esters on the thermal decomposition mechanism of GAP," J. Hazard. Mater. **154**, 112 (2008).
[29]A. Kramida, Yu. Ralchenko, J. Reader, and NIST ASD Team, *NIST Atomic Spectra Database (ver. 5.3)* (National Institute of Standards and Technology, Gaithersburg, MD, 2015), see http://physics.nist.gov/asd.
[30]C. M. Western, "PGOPHER: A program for simulating rotational, vibrational, and electronic spectra," J. Quant. Spectrosc. Radiat. Transfer **186**, 221 (2017).
[31]J. S. A. Brooke, P. F. Bernath, T. W. Schmidt, and G. B. Bacskay, "Line strengths and updated molecular constants for the C2 Swan system," J. Quant. Spectrosc. Radiat. Transfer **124**, 11 (2013).
[32]Ya. B. Zel'dovich and Yu. P. Raizer, *Physics of Shock Waves and High Temperature Hydrodynamic Phenomena* (Dover, New York, 2002), p. 99.
[33]H. Chang, X. Jin, and W. J. Zhou, "Experimental investigation of plume expansion dynamics of nanosecond laser ablated Al with small incidence angle," Optik **125**, 2923 (2014).
[34]R. B. Hall, "Laser production of blast waves in low pressure gases," J. Appl. Phys. **40**, 1941 (1969).
[35]J. C. Oxley, "The chemistry of explosives," in *Explosive Effects and Applications*, edited by J. A. Zukas and W. P. Walters (Springer, New York, 1998), pp. 137–172.